

TELKOMNIKA, Vol.16, No.6, December 2018, pp.2930–2942

ISSN: 1693-6930, accredited First Grade by Kemenristekdikti, Decree No: 21/E/KPT/2018

DOI: 10.12928/TELKOMNIKA.v16i6.9647

■ 2930

Sensorless Control of a Fault-tolerant Multi-level PMSM Drive

Kamel Saleh*, Mark SumnerAn-Najah National University, Nottingham University,
Palestine, United Kingdom*Corresponding author, e-mail: kamel.saleh@najah.edu

Abstract

This paper presents a new technique to track the saliency position in a permanent magnet synchronous motor (PMSM) post a single phase open-circuit fault. The PMSM is driven by a fault-tolerant multi-level inverter that is utilized to implement a fault-tolerant control strategy to minimize system performance degradation post the fault. The fault-tolerant multi-level inverter is consisting of a number of insulated-gate bipolar transistors (IGBTs). The dynamic current responses of the PMSM motor due to the switching actions of these IGBTs are used to extract the saliency position. This process is not introducing any modification to the operation of the fault-tolerant multi-level inverter as it uses only the fundamental pulse width modulation (PWM) waveform. Moreover, it considers the modifications introduced to the PMSM motor and the multi-level inverter post the fault. Simulation results are provided to verify the effectiveness of the proposed strategy of saliency tracking of a PMSM motor driven by a fault-tolerant four-leg multi-level inverter over a wide range of speeds in the case of a single-phase open circuit fault.

Keywords: four-leg multi-level inverter, sensorless, single-phase open circuit, space vector pulse width modulation

Copyright © 2018 Universitas Ahmad Dahlan. All rights reserved.

1. Introduction

Sensorless control of motor drives has been widely researched for systems employing standard two-level inverters [1-6]. These techniques introduce a significant additional current distortion which causes audible noise, torque pulsations and increases the system losses. In the other hand, a Multi-level inverter can achieve a higher voltage and power capability with conventional switching devices compared to two-level inverter and is now used for high power drives [7-9]. The particular structure of some of these converters offers significant potential for improving sensorless control of motors, as they employ H-bridge circuits with a relatively low DC link voltage. [10-12] are introducing different techniques to achieve sensorless control of multi-level inverter drives in healthy mode i.e no open circuit fault. Under faulty conditions, a number of fault-tolerant strategies to control two-level motor drives [13-18] and multi-level motor drives [19-22] have been used to enhance system operation under open circuit phase faults in sensor mode. [23-24] introduced a four-leg two-level (PMSM) drive to track the saturation saliency in the case of single-phase open circuit faults. This paper is introducing a new method to track the saturation saliency in a surface mounted permanent magnet motor in case of an open circuit fault. This motor is driven by a four-leg multi-level inverter. The objective is to maintain continuous system operation with a satisfactory performance to meet the safety procedure for the whole system and increase the reliability of the system.

2. Research Method

2.1. Fault Tolerant Multi-level Four-leg Converter Drive Topology

The proposed fault-tolerant multi-level drive topology is shown in Figure 1. A new Leg (fourth leg) is added to the conventional multi-level inverter. The redundant fourth leg is permanently connected the motor neutral point. Under healthy operating conditions, the two IGBTs in this fourth leg will be inactivated making it redundant (not used). This will make the fault-tolerant multi-level inverter running as conventional three-leg multi-level as shown in Figure 2. When a single phase open-circuit fault is introduced to one phase of the PMSM motor, the switches on the faulty phase are disabled and the IGBTs the fourth leg are immediately activated in order to control the voltage at the neutral point of the motor.

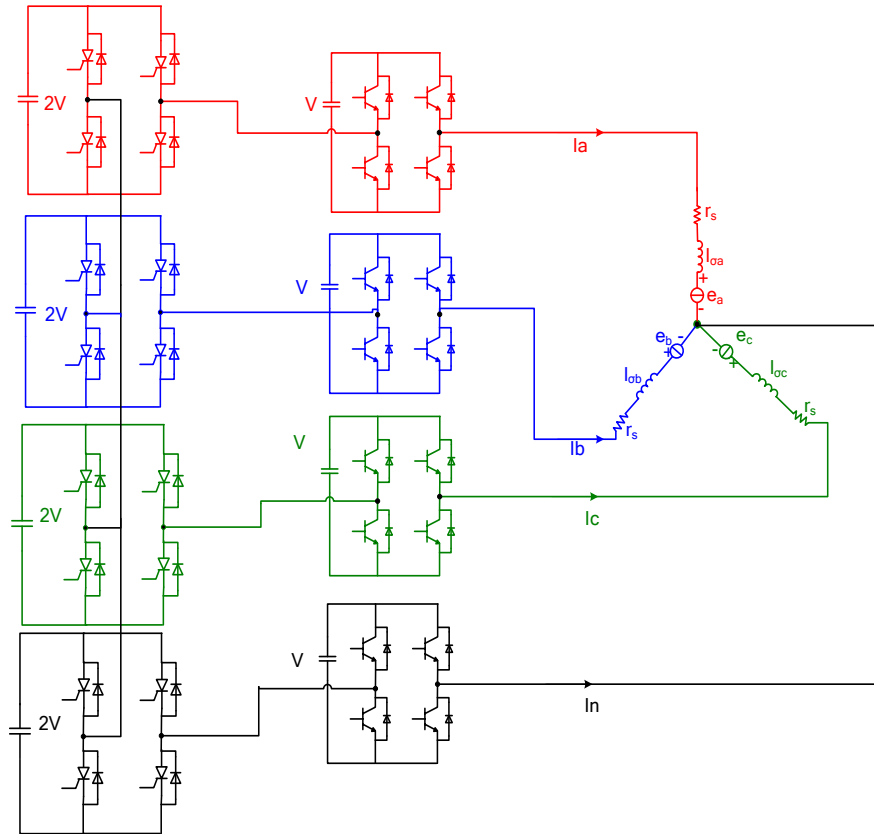


Figure 1. Four-leg asymmetric cascaded H-Bridge seven level converter

2.2. Healthy Operation of the Multi-level Inverter

The seven-level cascaded H-bridge inverter can generate the voltage $3V$, $2V$, V , 0 , $-V$, $-2V$ and $-3V$ from each leg as shown in Figure 2. According to the switching state of each cell in the multilevel converter, it is possible to generate 2^7 switching states (vector in space). These vectors can be transformed into $\alpha\beta$ coordinates (60° coordinate system) according to the following (1), (2) as shown in Figure 3:

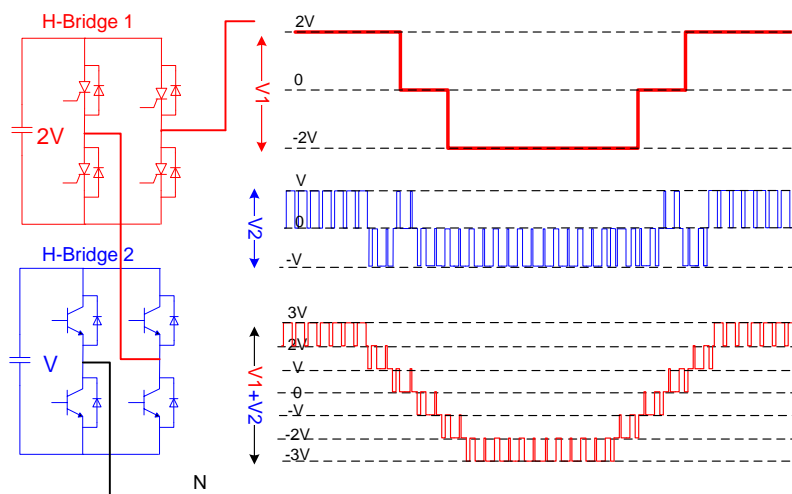


Figure 2. Operation of the seven level asymmetric hybrid cascaded H-bridge converter

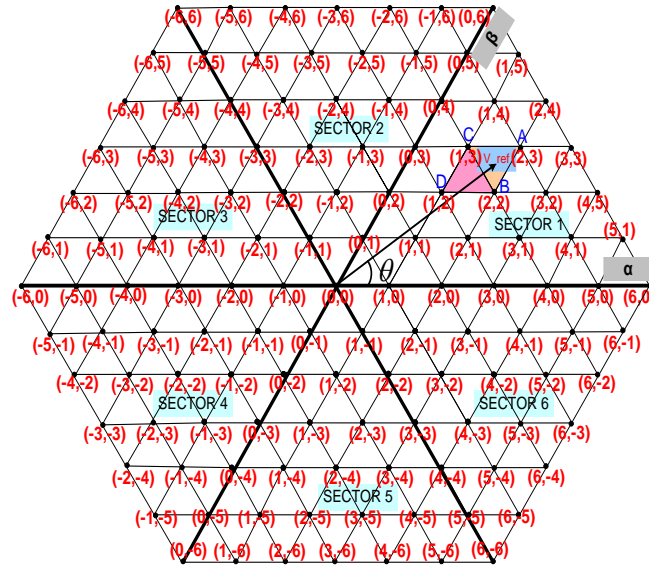


Figure 3. Seven level SVPWM state diagram in $\alpha\beta$ coordinates

$$V_{\alpha} = V \cos \theta - \frac{V \sin \theta}{\sqrt{3}} \quad (1)$$

$$V_{\beta} = \frac{2V \sin \theta}{\sqrt{3}} \quad (2)$$

where V_{α} and V_{β} are the coordinates of the vector V in the 60° coordinate system, V and θ are the amplitude and phase angle of the reference vector respectively. The whole modulation technique that is used in this paper when the motor is running under healthy operating condition is illustrated in [8].

2.3. Open Phase Fault Operation

To maintain the system performance after a single phase open-circuit fault is introduced to one phase of the motor, the rotating magnetomotive force should be maintained post the fault [18-24]. To do so, many modification should be introduced to the operation of the PMSM drive system. Firstly, the phase where the open circuit fault is introduced to should be isolated by disabling the IGBTs in that leg. This is achieved by setting the reference voltage of that phase to zero. Secondly the IGBTs in the Fourth leg should be activated immediately to make the zero sequence current to circulate through it. And Finally, the two remaining motor currents post the fault should be increased by a $\sqrt{3}$ as well as phase shifted 30 degrees away from the faulted phase compared to the currents generated under normal operation, as given in (3).

$$\begin{bmatrix} I_0 \\ I_b \\ I_c \end{bmatrix} = \begin{bmatrix} -\cos(\theta) & -\sin(\theta) \\ \sqrt{3} \cos(\theta - 150) & \sqrt{3} \sin(\theta - 150) \\ \sqrt{3} \sin(\theta - 150) & \sqrt{3} \sin(\theta + 150) \end{bmatrix} \begin{bmatrix} V_q \\ V_d \end{bmatrix} \quad (3)$$

These steps are illustrated in the vector control structure shown in Figure 4. It is assumed that an open-circuit fault is introduced to phase 'a' of the PMSM motor so that the current in phase 'a' drops to zero and the reference voltage of phase 'a' (V_a ref) is set to zero as well. Whereas the motor neutral current, which is the sum of the two remaining output currents (I_b and I_c), can circulate through the fourth phase of the multi-level inverter.

The simulation of the vector control structure shown in Figure 4 was carried out using SABER. Figure 5 shows the simulation results of a four-leg multi-level inverter PMSM drive system under healthy and faulted conditions. The motor was driving a 30 Nm load torque at 300 rpm speed and running under healthy operating condition. Then a successive speed steps are applied to the system till the speed reaches 1500 rpm. It is clear that the controller could

regulate the motor speed to follow the reference speed properly. The controlled currents i_d and i_q are stable at the reference levels while the motor currents are balanced 3-phase sinusoidal. At $t=1$ s, an open circuit fault is introduced to phase 'a'. At this time the switch of the fourth leg is activated, which means that the neutral is connected to the supply. Then different reference speed commands are applied to the system. The simulation results show that ripple in the torque is almost the same as under normal operating conditions. The currents i_d and i_q are now controlled properly.

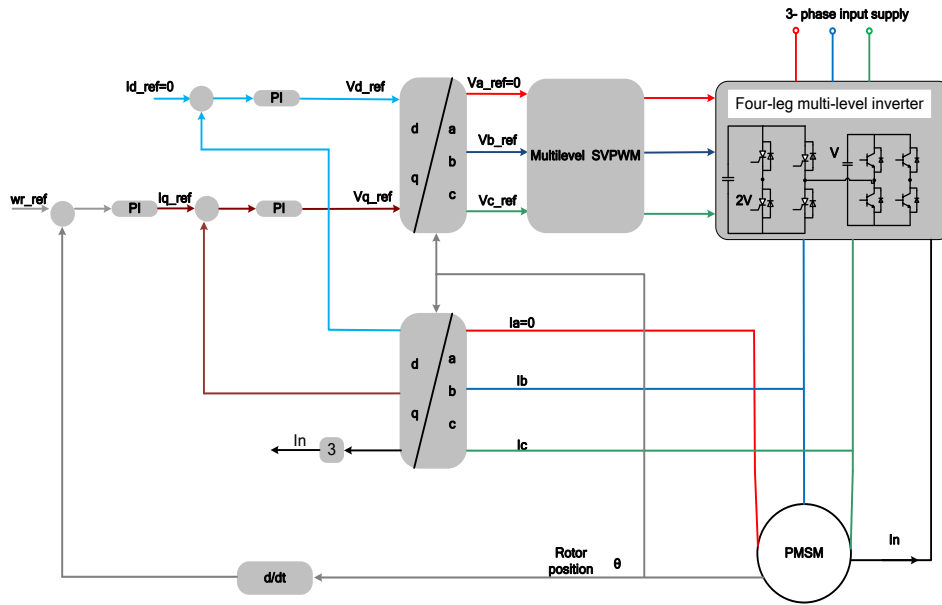


Figure 4. The vector control structure for the four-phase multi-level inverter PMSM drive under a phase 'a' open-circuit fault

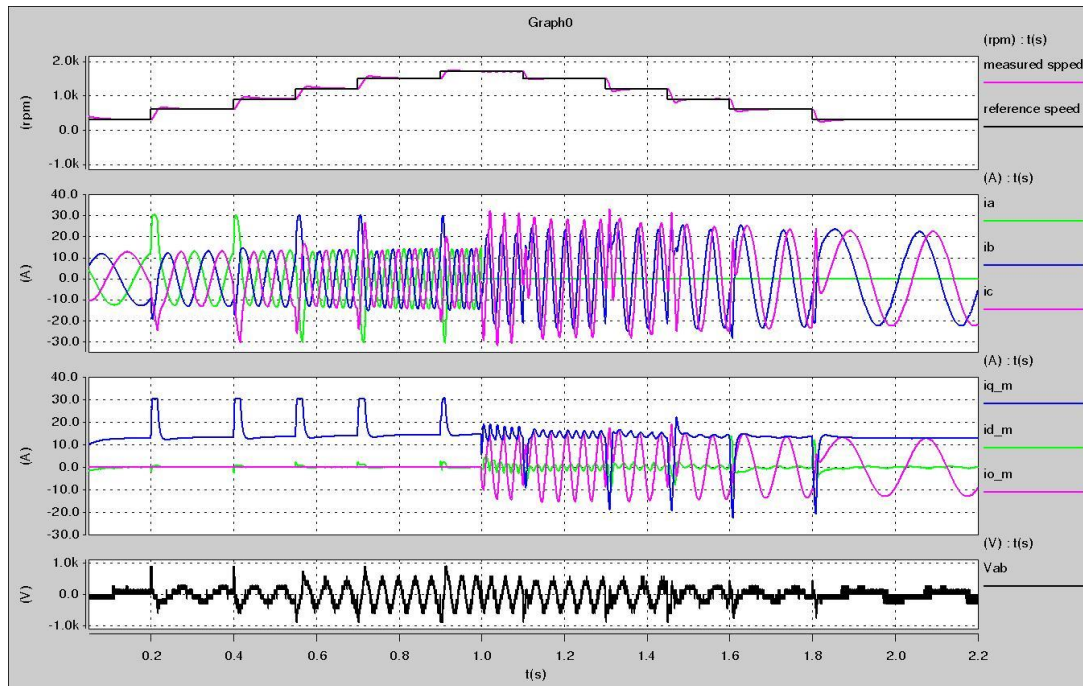


Figure 5 Performance of a 4-phase multi-level inverter PMSM drive system under different operating conditions

2.4. Tracking the Saturation Saliency of PMSM under Healthy Condition

The stator leakage inductances of the induction motor are modulated by anisotropy either from the rotor slotting or from the saturation of the main flux. The modulation can be expressed by the following (4) to (6).

$$l\sigma a = L_0 + \Delta L \cos(n_{an}\theta_{an}) \quad (4)$$

$$l\sigma b = L_0 + \Delta L \cos\left(n_{an}\left(\theta_{an} - \frac{2\pi}{3}\right)\right) \quad (5)$$

$$l\sigma c = L_0 + \Delta L \cos\left(n_{an}\left(\theta_{an} - \frac{4\pi}{3}\right)\right) \quad (6)$$

where L_0 is the average inductance and ΔL is the variation of leakage inductance due to the rotor anisotropy ($n_{an}=2$ for saturation anisotropy)

This modulation of the stator leakage inductances will be reflected in the transient response of the motor line current to the test vector imposed by the multi-level inverter. So by using the fundamental PWM wave form and by measuring the transient current response to the active vectors it is possible to detect the inductance variation and track the rotor position for three-leg multilevel inverter. After obtaining the scalar quantities p_a , p_b and p_c then the position of the saliency can be constructed as shown in (7).

$$\vec{p} = p_\alpha + jp_\beta = p_a + ap_b + a^2p_c \quad (7)$$

The algorithm to track the saliency in 3-leg multi-level inverter that is proposed in [9] is used to track the saliency for four-leg multilevel inverter and the results is shown in Figure 6. Under the healthy operation, the switches in the fourth leg will not be activated and so the algorithm proposed in [9] could track the saliency from $t=0.1$ s till $t=1$ s at different speeds. In case of an open phase fault ($t=1$ s to 2.2s), the algorithm is no longer able to track the saliency as shown in Figure 6. This because the measurement of the current response (di/dt) associated with the faulty phase will become zeros as $i_a=0$. Which means that these position scalars will be zero as seen in Figure 6.

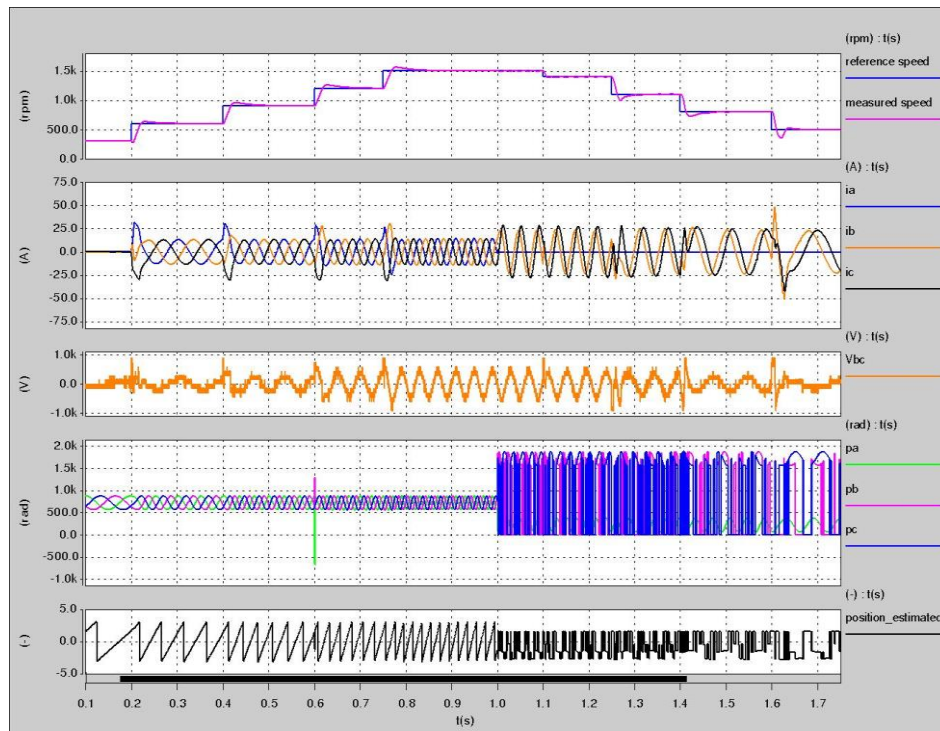


Figure 6. Tracking the saturation saliency in healthy mode and phase a open circuit case

2.5. Tracking the Saliency in Multilevel Inverter under Unhealthy Condition

Figure 7 shows the Type0 switching sequence of the four-leg multi-level inverter under phase 'a' open circuit fault and activating the fourth leg. The stator circuit when the vectors V1, V2 and V0 are applied are shown in Figure 8 (a), 8 (b) and 8 (c) respectively.

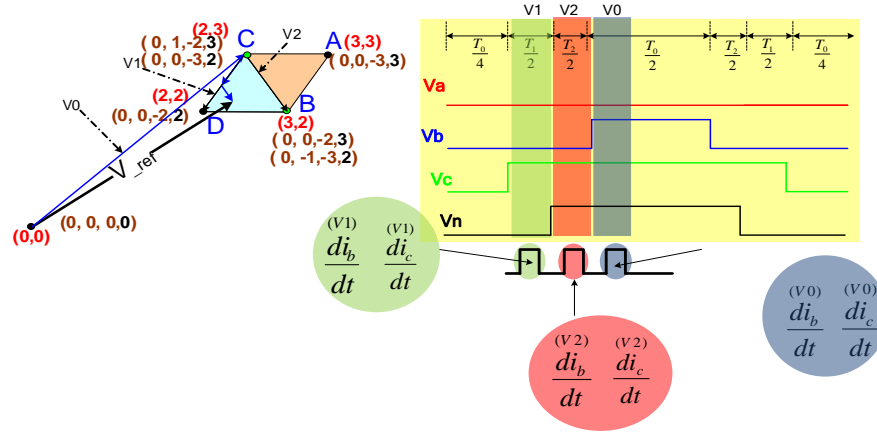


Figure 7. Switching sequence for Type0 in sector 1 in the multi-level space diagram under phase a open circuit fault and the fourth leg is activated

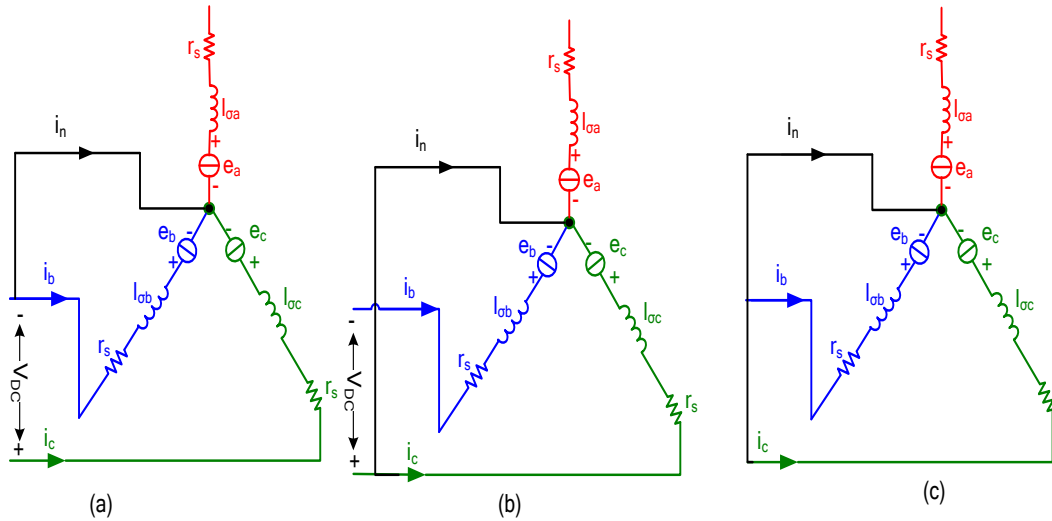


Figure 8. Stator circuits when: (a) V1 is applied; (b) V2 is applied; (c) V0 is applied

Using the circuit in Figure 8 (a), the following equations hold true:

$$0 = r_s * i_b^{(V1)} + l_{sb} * \frac{di_b^{(V1)}}{dt} + e_b^{(V1)} \quad (8)$$

$$V_{DC} = r_s * i_c^{(V1)} + l_{sc} * \frac{di_c^{(V1)}}{dt} + e_c^{(V1)} \quad (9)$$

the following equations are obtained using Figure 8 (b):-

$$-V_{DC} = r_s * i_b^{(V2)} + l_{sb} * \frac{di_b^{(V2)}}{dt} + e_b^{(V2)} \quad (10)$$

$$0 = r_s * i_c^{(V2)} + l_{\sigma c} * \frac{di_c^{(V2)}}{dt} + e_c^{(V2)} \quad (11)$$

finally when V_0 is applied as shown in Fig 8 (c), the following equations hold true:

$$0 = r_s * i_b^{(V0)} + l_{\sigma b} * \frac{di_b^{(V0)}}{dt} + e_b^{(V0)} \quad (12)$$

$$0 = r_s * i_c^{(V0)} + l_{\sigma c} * \frac{di_c^{(V0)}}{dt} + e_c^{(V0)} \quad (13)$$

Assuming that the voltage drop across the stator resistances are small and can be neglected and the back emf can be cancelled if the time separation between the vectors is small. Subtracting (12) from (10) and (13) from (9) respectively yields:

$$-V_{DC} = l_{\sigma b} * \left(\frac{di_b^{(V2)}}{dt} - \frac{di_b^{(V0)}}{dt} \right) \quad (14)$$

$$-V_{DC} = l_{\sigma c} * \left(\frac{di_c^{(V0)}}{dt} - \frac{di_c^{(V1)}}{dt} \right) \quad (15)$$

Finally:

$$P_b = l_{\sigma b} * \left(\frac{di_b^{(V2)}}{dt} - \frac{di_b^{(V0)}}{dt} \right) \quad (16)$$

$$P_c = l_{\sigma c} * \left(\frac{di_c^{(V0)}}{dt} - \frac{di_c^{(V1)}}{dt} \right) \quad (17)$$

P_a can't be obtained from measuring the current response in phase a as it is zero in the case of an open circuit phase fault. But it can be deduced from P_b and P_c according to the following (18):

$$P_a = P_b - P_c \quad (18)$$

By doing the same procedures for other sectors, Tables 1 to 6 can be constructed to track the saliency in case of phase 'a' open circuit. Figure 9 shows the results of the simulation after modifying the tracking saliency algorithm as introduced in Tables 1 to 6. The figure shows that the new algorithm can track the saliency in the case of an open-circuit fault is introduced to phase 'a' fault with the same quality as in healthy conditions.

Table 1. Selection of p_a , p_b , and p_c in Sector 1 for a Star-connected Machine Driven by 4-leg Multi-level Inverter in Case of Phase a Open Circuit Fault

Sector 1					
Triangle	Vectors	P_a	P_b	P_c	
Type0 ΔBCD	V_1, V_2, V_0	$-(P_b - P_c)$	$\left(\frac{di_b^{(V2)}}{dt} - \frac{di_b^{(V0)}}{dt} \right)$	$\left(\frac{di_c^{(V0)}}{dt} - \frac{di_c^{(V1)}}{dt} \right)$	
Type1 ΔBCA	V_1, V_2, V_0	$-(P_b - P_c)$	$\left(\frac{di_b^{(V2)}}{dt} - \frac{di_b^{(V0)}}{dt} \right)$	$\left(\frac{di_c^{(V1)}}{dt} - \frac{di_c^{(V2)}}{dt} \right)$	
Type 2 ΔBCD	$V_1 + V_0$	$-(P_b - P_c)$	$\left(\frac{di_b^{(V1)}}{dt} - \frac{di_b^{(V2)}}{dt} \right)$	$\left(\frac{di_c^{(V2)}}{dt} - \frac{di_c^{(V0)}}{dt} \right)$	
Type 3 ΔBCA	$V_1 + V_0$	$-(P_b - P_c)$	$\left(\frac{di_b^{(V1)}}{dt} - \frac{di_b^{(V2)}}{dt} \right)$	$\left(\frac{di_c^{(V2)}}{dt} - \frac{di_c^{(V0)}}{dt} \right)$	

Table 2. Selection of p_a , p_b , and p_c in sector 2 for a star-connected Machine Driven by 4-leg Multi-level Inverter in Case of Phase a Open Circuit Fault

Triangle	Vectors	Sector 2			
		P_a	P_b		P_c
Type0 ΔBCD	V_1, V_2, V_0	$-(P_b - P_c)$	$(\frac{d i_b^{(V1)}}{dt} - \frac{d i_b^{(V0)}}{dt})$	$(\frac{d i_c^{(V2)}}{dt} - \frac{d i_c^{(V1)}}{dt})$	
Type1 ΔBCA	V_1, V_2, V_0	$-(P_b - P_c)$	$(\frac{d i_b^{(V2)}}{dt} - \frac{d i_b^{(V1)}}{dt})$	$(\frac{d i_c^{(V1)}}{dt} - \frac{d i_c^{(V0)}}{dt})$	
Type 2 ΔBCD	$V_1 + V_0$	$-(P_b - P_c)$	$(\frac{d i_b^{(V0)}}{dt} - \frac{d i_b^{(V2)}}{dt})$	$(\frac{d i_c^{(V1)}}{dt} - \frac{d i_c^{(V0)}}{dt})$	
Type 3 ΔBCA	$V_1 + V_0$	$-(P_b - P_c)$	$(\frac{d i_b^{(V1)}}{dt} - \frac{d i_b^{(V0)}}{dt})$	$(\frac{d i_c^{(V0)}}{dt} - \frac{d i_c^{(V2)}}{dt})$	

Table 3. Selection of p_a , p_b , and p_c in Sector 3 for a Star-connected Machine Driven by 4-leg Multi-level Inverter in case of Phase a Open Circuit Fault

Triangle	Vectors	Sector 3			
		P_a	P_b		P_c
Type0 ΔBCD	V_1, V_2, V_0	$-(P_b - P_c)$	$(\frac{d i_b^{(V1)}}{dt} - \frac{d i_b^{(V2)}}{dt})$	$(\frac{d i_c^{(V2)}}{dt} - \frac{d i_c^{(V0)}}{dt})$	
Type1 ΔBCA	V_1, V_2, V_0	$-(P_b - P_c)$	$(\frac{d i_b^{(V0)}}{dt} - \frac{d i_b^{(V1)}}{dt})$	$(\frac{d i_c^{(V2)}}{dt} - \frac{d i_c^{(V0)}}{dt})$	
Type 2 ΔBCD	$V_1 + V_0$	$-(P_b - P_c)$	$(\frac{d i_b^{(V0)}}{dt} - \frac{d i_b^{(V1)}}{dt})$	$(\frac{d i_c^{(V1)}}{dt} - \frac{d i_c^{(V2)}}{dt})$	
Type 3 ΔBCA	$V_1 + V_0$	$-(P_b - P_c)$	$(\frac{d i_b^{(V2)}}{dt} - \frac{d i_b^{(V0)}}{dt})$	$(\frac{d i_c^{(V1)}}{dt} - \frac{d i_c^{(V2)}}{dt})$	

Table 4. Selection of p_a , p_b , and p_c in Sector 4 for a Star-connected Machine Driven by 4-leg Multi-level Inverter in case of Phase a Open Circuit Fault

Triangle	Vectors	Sector 4			
		P_a	P_b		P_c
Type0 ΔBCD	V_1, V_2, V_0	$-(P_b - P_c)$	$(\frac{d i_b^{(V0)}}{dt} - \frac{d i_b^{(V2)}}{dt})$	$(\frac{d i_c^{(V1)}}{dt} - \frac{d i_c^{(V0)}}{dt})$	
Type1 ΔBCA	V_1, V_2, V_0	$-(P_b - P_c)$	$(\frac{d i_b^{(V0)}}{dt} - \frac{d i_b^{(V2)}}{dt})$	$(\frac{d i_c^{(V2)}}{dt} - \frac{d i_c^{(V1)}}{dt})$	
Type 2 ΔBCD	$V_1 + V_0$	$-(P_b - P_c)$	$(\frac{d i_b^{(V2)}}{dt} - \frac{d i_b^{(V1)}}{dt})$	$(\frac{d i_c^{(V0)}}{dt} - \frac{d i_c^{(V2)}}{dt})$	
Type 3 ΔBCA	$V_1 + V_0$	$-(P_b - P_c)$	$(\frac{d i_b^{(V2)}}{dt} - \frac{d i_b^{(V1)}}{dt})$	$(\frac{d i_c^{(V1)}}{dt} - \frac{d i_c^{(V0)}}{dt})$	

Table 5. Selection of pa, pb, and pc in Sector 5 for a Star-connected Machine Driven by 4-leg Multi-level Inverter in Case of Phase a Open Circuit Fault

Sector 5				
Triangle	Vectors	Pa	Pb	Pc
Type0 ΔBCD	V1,V2,Vo	$-(P_b - P_c)$	$(\frac{di_b^{(V0)}}{dt} - \frac{di_b^{(V1)}}{dt})$	$(\frac{di_c^{(V1)}}{dt} - \frac{di_c^{(V2)}}{dt})$
Type1 ΔBCA	V1,V2,Vo	$-(P_b - P_c)$	$(\frac{di_b^{(V1)}}{dt} - \frac{di_b^{(V2)}}{dt})$	$(\frac{di_c^{(V0)}}{dt} - \frac{di_c^{(V1)}}{dt})$
Type 2 ΔBCD	V1+Vo	$-(P_b - P_c)$	$(\frac{di_b^{(V2)}}{dt} - \frac{di_b^{(V0)}}{dt})$	$(\frac{di_c^{(V0)}}{dt} - \frac{di_c^{(V1)}}{dt})$
Type 3 ΔBCA	V1+Vo	$-(P_b - P_c)$	$(\frac{di_b^{(V0)}}{dt} - \frac{di_b^{(V1)}}{dt})$	$(\frac{di_c^{(V2)}}{dt} - \frac{di_c^{(V0)}}{dt})$

Table 6. Selection of pa, pb, and pc in Sector 6 for a Star-connected Machine Driven by 4-leg Multi-level Inverter in Case of Phase a Open Circuit Fault

Sector 6				
Triangle	Vectors	Pa	Pb	Pc
Type0 ΔBCD	V1,V2,Vo	$-(P_b - P_c)$	$(\frac{di_b^{(V2)}}{dt} - \frac{di_b^{(V1)}}{dt})$	$(\frac{di_c^{(V0)}}{dt} - \frac{di_c^{(V2)}}{dt})$
Type1 ΔBCA	V1,V2,Vo	$-(P_b - P_c)$	$(\frac{di_b^{(V2)}}{dt} - \frac{di_b^{(V1)}}{dt})$	$(\frac{di_c^{(V0)}}{dt} - \frac{di_c^{(V2)}}{dt})$
Type 2 ΔBCD	V1+Vo	$-(P_b - P_c)$	$(\frac{di_b^{(V1)}}{dt} - \frac{di_b^{(V0)}}{dt})$	$(\frac{di_c^{(V2)}}{dt} - \frac{di_c^{(V1)}}{dt})$
Type 3 ΔBCA	V1+Vo	$-(P_b - P_c)$	$(\frac{di_b^{(V0)}}{dt} - \frac{di_b^{(V2)}}{dt})$	$(\frac{di_c^{(V2)}}{dt} - \frac{di_c^{(V1)}}{dt})$

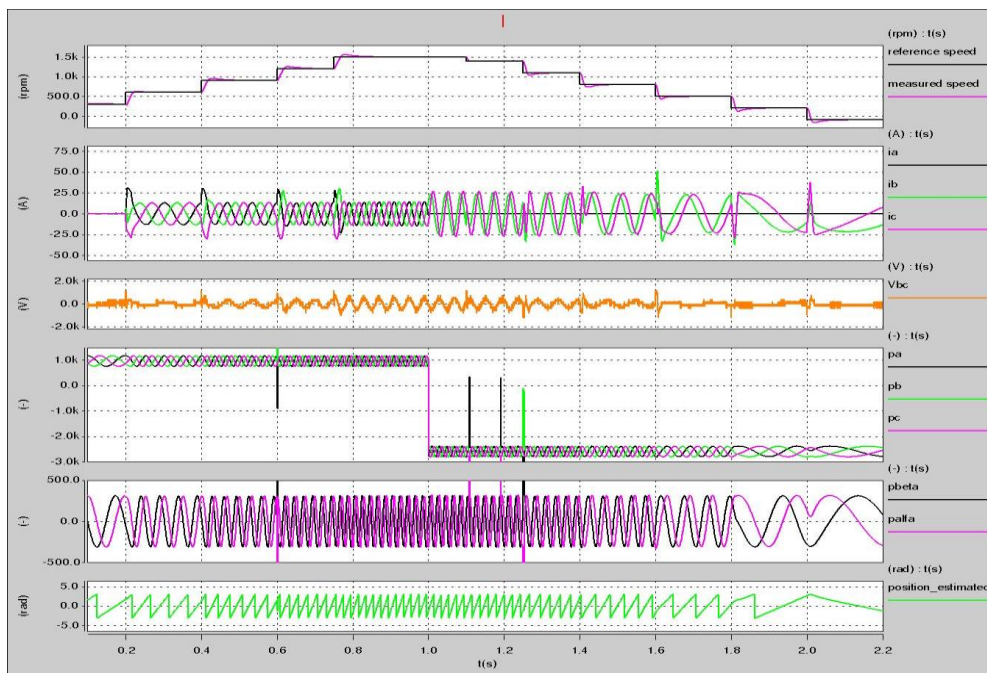


Figure 9. The algorithm to track the saliency in of multilevel inverter using the fundamental PWM algorithm given in [12] for healthy mode and the algorithm presented above for unhealthy condition

3. Results and Analysis

3.1. The Sensorless Vector Control Structure

The sensorless speed control for PMSM motor driven by a fault-tolerant multi-level inverter has been implemented in simulation in the SABER modeling environment. The saturation saliency position signal $P\alpha\beta$ are used as the input to a mechanical observer [25] to obtain a filtered signal for the estimated speed ω^\wedge and a cleaned position θ^\wedge . Note that the simulation includes a minimum pulse width of 10 μ s when di/dt measurements are made, similar to the experimental results of [6]. This estimated speed ω^\wedge and position θ^\wedge are used to obtain a fully sensorless speed control as shown in Figure 10.

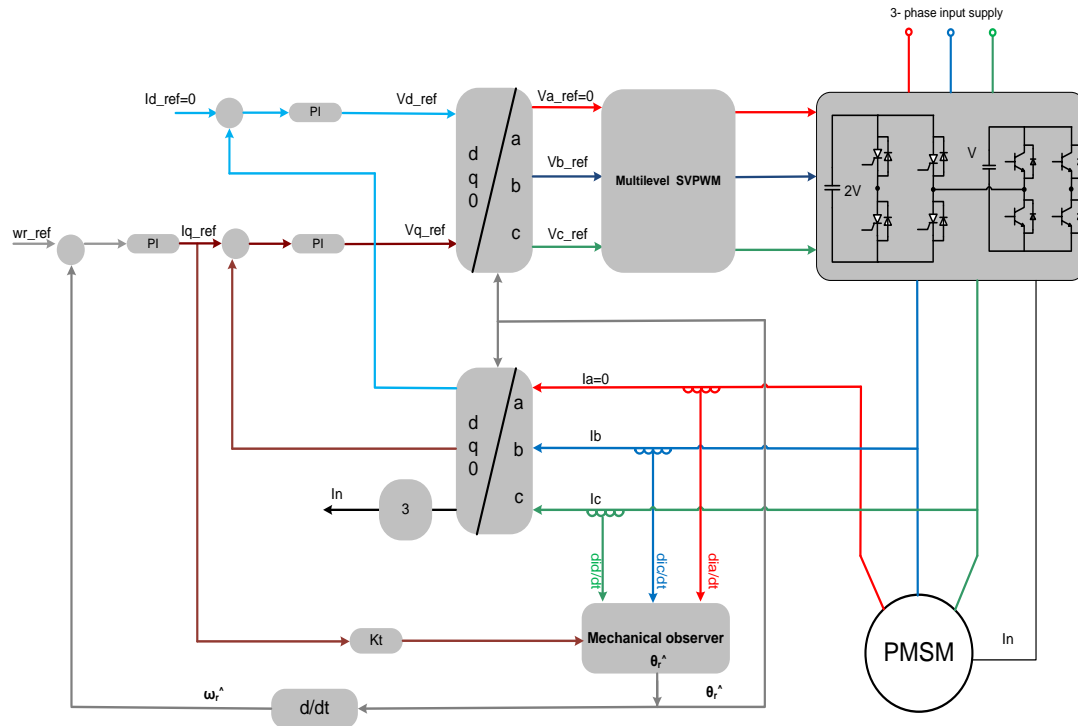


Figure 10. The sensorless vector control structure for the 4-leg multi-level inverter PMSM drive under a phase a open-circuit fault

3.2. Fully Sensorless Speed Control of Four-leg Multilevel Inverter

Figure 11 shows the results of a fully sensorless speed control of a PMSM motor driven by a fault-tolerant multi-level inverter at loaded condition using the algorithm proposed in [12] for the healthy case and the method proposed above in the case of phase 'a' open circuit fault. The results of this test illustrate the capability of the PMSM motor drive system to work at very low and zero speeds in healthy operating condition and when a single phase open-circuit fault is introduced to the operation of the motor. The motor was working in sensorless healthy mode at speed 30 rpm, and then at time $t=7.5$ s a speed step change from 30 rpm to 0 rpm (until $t=9$ s) is applied to the system. Figure 11 shows that the motor responded to the speed step with a good transient and steady state response. At time $t=9$ s, an open circuit fault in phase a was introduced to the system, and this can be noticed from $I_a \neq 0$ and the current waveforms ($I_a=0$, I_b , and I_c are multiplied by $\sqrt{3}$ and shifted by 60 degrees). Figure 11 shows that performance of the whole system under faulty conditions is in the same level of performance in healthy mode. Moreover, the motor responded to a speed step from 0 rpm to 30 rpm at $t=10.5$ s with acceptable transient and steady state performance.

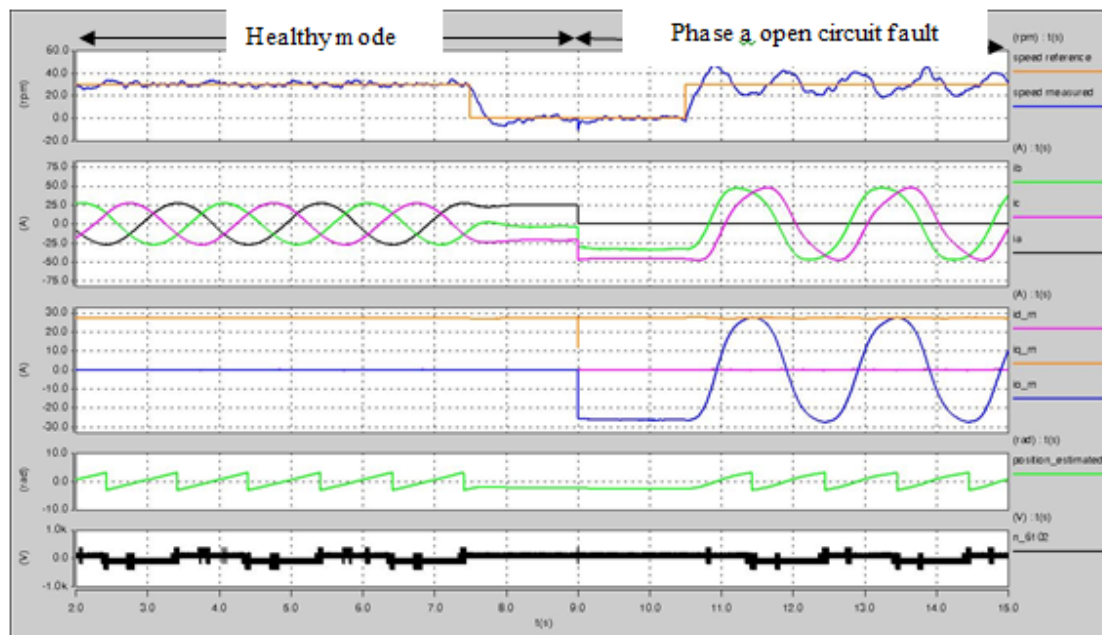


Figure 11. Fully sensorless speed steps between 0.5 Hz, 0 to 0.5 Hz, half under healthy condition and half under open phase a fault condition

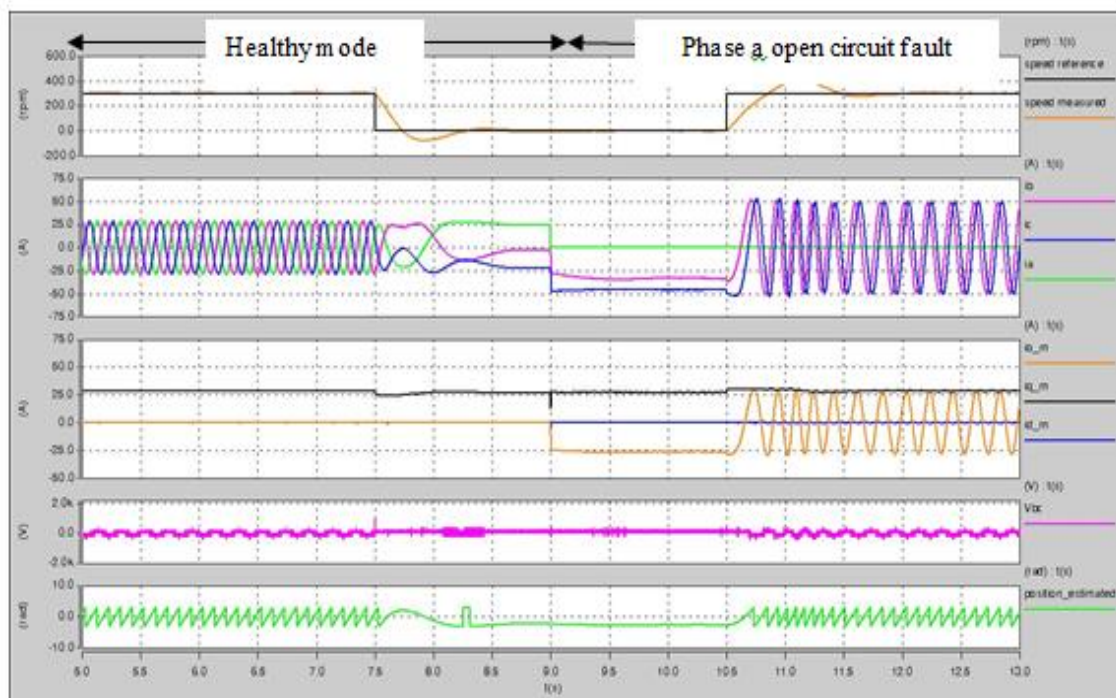


Figure 12. Fully sensorless speed steps between 10 Hz, 0 to 10 Hz, half under healthy condition and half under open phase a fault condition

Figure 13 demonstrates the stability of the fully sensorless system when a load disturbance is applied at low speed (30 rpm) in both healthy mode and under phase fault conditions. The results show that the system maintains the speed in all the cases.

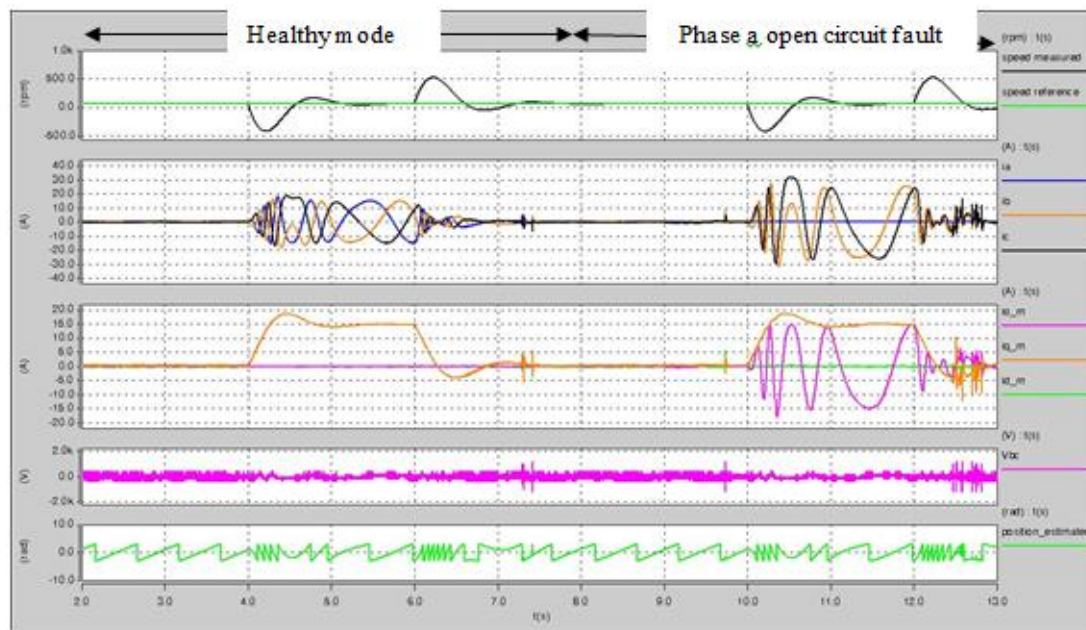


Figure 13. Fully sensorless half load steps under healthy condition and under open phase a fault condition

4. Conclusion

This paper has outlined a new scheme for tracking the saliency of a motor fed by a four-leg multi-level inverter in the case of a single phase open circuit fault through measuring the dynamic current response of the motor line currents due to the IGBT switching actions. The proposed method includes software modification to the method proposed in [12] to track the saliency of the motor under healthy conditions to make it applicable in the cases of open circuit phase condition. The new strategy can be used to track the saturation saliency in PM motors (2 fe) and the rotor slotting saliency in IMs (14*fr) similar to the method used in a healthy motor drive and the only difference between the PM and IM will be the tracked harmonic number. The results have shown the effectiveness of the new method in increasing the safety measures in critical systems that need continuous operation. The drawbacks of this method are increasing the total harmonic distortion of the motor's current, especially at a very low speed, due to the minimum pulse width in addition to the need for 3 di/dt sensors.

References

- [1] Jansen PL, Lorenz RD. Transducerless position and velocity estimation in induction and salient AC machines. *IEEE T Ind Appl* 1995; 31:240–247.
- [2] Jung-IkH, OhtoM, Ji-Hoon J, Seung-Ki S. *Design and selection of AC machines for saliency-based sensorless control*. In: IEEE2002Industrial Applications Conference. Pittsburgh, USA. NewYork, NY, USA: IEEE. 13-18 October 2002: 1155–1162.
- [3] Linke M, Kennel R, Holtz J. *Sensorless speed and position control of synchronous machines using alternating carrier injection*. In: IEEE 2003 International Electric Machines and Drives Conference. Wisconsin, USA. New York, NY, USA: IEEE. 1-4 June 2003: 1211–1217.
- [4] Schroedl M. *Sensorless control of AC machines at low speed and standstill based on the INFORM method*. In: IEEE 1996 Industry Applications Conference. San Diego, USA. New York, NY, USA: IEEE. 6 -10 October 1996: 270-277.
- [5] HoltzJ, Juliet J. *Sensorless acquisition of the rotor position angle of induction motors with arbitrary stator winding*. In: IEEE 2004 Industry Applications Conference. Washington, USA. NewYork, NY, USA: IEEE. ; 3-7 October 2004: 1321-1328.
- [6] Qiang G, Asher GM, Sumner M, Makys P. *Position estimation of AC machines at all frequencies using only space vector PWM based excitation*. In: IET 2006 International Conference on Power Electronics, Machines and Drives. Dublin, Ireland. Savoy Place, London, UK: IET. 4-6 April 2006: 61-70

- [7] MD Manjrekar, PK Steimer, TA Lipo. Hybrid Multilevel Power Conversion System: A competitive Solution for High-Power Applications. *IEEE transactions on industry applications*. 2000; 36: 834-841.
- [8] Sanmin Wei, Bin Wu, Qianghua Wang. *An Improved Space Vector PWM Control Algorithm for Multilevel Inverters*. Power Electronics and Motion Control Conference. Aug, 2004; 3: 1124-1129.
- [9] K Saleh, GM Asher, M Sumner, M Tomasini, G Qiang. Low Speed Sensorless Control of an Induction Motor Fed by Multilevel Converter to Reduce Current Distortion. 13th European Conference on Power Electronics and Applications. Barcelona. 2009.
- [10] Jie Zhang. *Speed sensorless AC drive fed by three-level inverter with full-dimensional spiral vector control for improved low-speed performance*. Industry Applications Conference, 1996. Thirty-First IAS Annual Meeting, IAS '96. Conference Record of the 1996 IEEE, San Diego, CA, 1996; 1: 243-249.
- [11] O Chandra Sekhar, K Chandra sekhar. A novel five-level inverter topology for DTC induction motor drive. 2012 IEEE International Conference on Advanced Communication Control and Computing Technologies (ICACCCT), Ramanathapuram. 2012: 392-396.
- [12] K Saleh, M Sumner. Modelling and Simulation of a Sensorless Control of a True Asymmetric Cascade H-Bridge Multilevel Inverter PMSM Drives. *International Journal of Power Electronics and Drive System (IJPEDS)*. June 2016; 7(2): 397-415.
- [13] MS Mendes, AJ Cardoso. Fault-tolerant operating strategies applied to three-phase induction motor drives. *IEEE Transaction on Industrial Electronic*. 2006; 53: 1807-1817.
- [14] N Bianchi, S Bolognani, M Zigliotto, M Zordan. Innovative remedial strategies for inverter faults in IPM synchronous motor drives. *IEEE Transaction on Energy Conversion*. 2003; 18: 306-314.
- [15] F Meinguet, J Gyselinck. *Control strategies and reconfiguration of four-leg inverter PMSM drives in case of single-phase open-circuit faults*. IEEE International Electric Machines and Drives Conference, Miami, FL. 2009: 299-304.
- [16] S Kwak, T Kim, O Vodyakho. *Four-leg based Matrix Converter with Fault Resilient Structures and Controls for Electric Vehicle and Propulsion Systems*. IEEE Vehicle Power and Propulsion Conference, Arlington, TX. 2007: 519-523.
- [17] BA Welchko, TA Lipo, TM Jahns, SE Schulz. Fault tolerant three-phase ac motor drive topologies: a comparison of features, cost, and limitation. *IEEE Transaction o Power Electronic*. 2004; 19: 1108-1116.
- [18] S Khwan On, L De Lillo, PW Wheeler, L Empringham. *Fault tolerant four-leg matrix converter motor drive topologies for aerospace applications*. in Proc. IEEE ISIE. 2010: 2166–2171.
- [19] Mohammad Ali Paymani, Mohammad Saleh Marhaba, H Iman Eini. *Fault-tolerant operation of a medium voltage drive based on the Cascaded H-bridge inverter*. 2011 2nd Power Electronics, Drive Systems and Technologies Conference, Tehran. 2011: 551-556.
- [20] G Grandi, P Sanjeevikumar, Y Gritli, F Filippetti. Experimental investigation of fault-tolerant control strategies for quad-inverter converters. *Electrical Systems for Aircraft*. Railway and Ship Propulsion, Bologna, 2012: 1-8.
- [21] M Alavi, D Wang, M Luo. *Model-based diagnosis and fault tolerant control for multi-level inverters*. IECON 2015-41st Annual Conference of the IEEE Industrial Electronics Society, Yokohama, 2015: 001548-001553.
- [22] K Thanirige, SK Panda, AK Rathore, S Mukherjee, MA Zagrodnik, AK Gupta, *Fault-tolerant cascaded multi-level inverter with improved output quality*. 2016 IEEE International Conference on Sustainable Energy Technologies (ICSET), Hanoi. 2016: 332-337.
- [23] K Saleh, M Sumner. Modeling and simulation of sensorless control of four-leg inverter PMSM drives in the case of a single-phase open circuit fault. *Turkish Journal of Electrical Engineering & Computer Sciences*. 2016; 24: 3807-3820.
- [24] K Saleh, M Sumner. *Sensorless Control of a Fault Tolerant PMSM Drives in Case of Single-phase Open Circuit Fault*. International Symposium on Power Electronics, Electrical Drives, Automation and Motion (SPEEDAM). 2016; 7:1061-1074.
- [25] Lorenz RD, Van Patten KW. High-resolution velocity estimation for all-digital, ac servo drives. *IEEE Transaction in Industrial Applications*. 1991; 27: 701-705.